nature climate change

LETTERS

PUBLISHED ONLINE: 11 NOVEMBER 2012 | DOI: 10.1038/NCLIMATE1732

Response of snow-dependent hydrologic extremes to continued global warming

Noah S. Diffenbaugh[1]*, Martin Scherer[1] and Moetasim Ashfaq[2]

Snow accumulation is critical for water availability in the Northern Hemisphere[1,2], raising concern that global warming could have important impacts on natural and human systems in snow-dependent regions[1,3]. Although regional hydrologic changes have been observed (for example, refs 1,3–5), the time of emergence of extreme changes in snow accumulation and melt remains a key unknown for assessing climate-change impacts[3,6,7]. We find that the CMIP5 global climate model ensemble exhibits an imminent shift towards low snow years in the Northern Hemisphere, with areas of western North America, northeastern Europe and the Greater Himalaya showing the strongest emergence during the near-term decades and at 2 °C global warming. The occurrence of extremely low snow years becomes widespread by the late twenty-first century, as do the occurrences of extremely high early-season snowmelt and runoff (implying increasing flood risk), and extremely low late-season snowmelt and runoff (implying increasing water stress). Our results suggest that many snow-dependent regions of the Northern Hemisphere are likely to experience increasing stress from low snow years within the next three decades, and from extreme changes in snow-dominated water resources if global warming exceeds 2 °C above the pre-industrial baseline.

Water resources in most land areas north of 30° N are dependent on natural water storage provided by snowpack[1,2], with water accumulated in the solid phase during the cold season and released in the liquid phase during warm events and the warm season. Abnormally warm conditions increase the fraction of accumulated snow that melts and the fraction of precipitation that falls as rain, resulting in low seasonal snow accumulation, high cold-season surface runoff and low warm-season surface runoff[3]. Such events exert stress on a wide array of natural and human systems, including through increased pest pressure[8], wild fires[9] and die-off[10] in forest ecosystems; decreased water supply for agriculture, energy generation, human consumption and riparian ecosystems[2,11,12]; and decreased snow availability for recreation[13]. Given these vulnerabilities and the critical sensitivity of snow to temperature, global warming is expected to impact natural and human systems in snow-dependent regions[1,3,13]. However, because internal climate system variability strongly influences cold-season temperature and precipitation[14,15], the pattern of emergence of robust changes in the extremes of snow accumulation and melt remains an important uncertainty for both adaptation and mitigation decisions[3].

We analyse snow-related variables from the CMIP5 Representative Concentration Pathway 8.5(RCP8.5) global climate model experiment[16] (see Methods). Of the Intergovernmental Panel on Climate Change RCPs, RCP8.5 exhibits the highest levels of forcing and global warming at the end of the twenty-first century, with radiative forcing reaching ~8.5 W m^{-2}, greenhouse-gas concentrations exceeding 1,370 ppm CO_2-e (ref. 17) and median global warming reaching 4.9 °C above the pre-industrial baseline[18].

Given the importance of 1 April snow water equivalent[7,19,20] (SWE), we focus our snow accumulation analyses on the monthly mean March SWE (see Methods). Although the CMIP5 ensemble captures the observed geographic distribution of snow occurrence[1] (Supplementary Fig. S1), the ensemble shows substantial biases in the simulated baseline March SWE, with all nine of our illustrative regions exhibiting at least a half order of magnitude range in model agreement with the observational mean and/or interannual variability (Fig. 1; see Methods for description of the observational snow data). However, in spite of the substantial disagreement with observations, there is substantial agreement in the simulated fraction of March SWE remaining during all three twenty-first-century periods, with the ensemble mean exceeding 2 standard deviations of the ensemble variability in all nine regions (except the western US in 2070–2099 and central Asia in 2040–2069 and 2070–2099; Fig. 1 and Supplementary Figs S2 and S3).

The fact that the CMIP5 ensemble exhibits a robust response of regional snow accumulation to elevated greenhouse forcing motivates exploration of potential changes in snow-related hydrologic extremes. We begin by analysing the percentage of years in which March SWE falls below the simulated 1976–2005 median value (low years) and minimum value (extremely low years; Fig. 2). The occurrence of low years intensifies throughout most snow-dominated areas[1] of the Northern Hemisphere during the twenty-first century, reaching greater than 80% over most of North America, western Eurasia and southeastern Eurasia during the 2070–2099 period. The areas of North America and Eurasia that exhibit peak occurrence of low snow years also exhibit peak occurrence of extremely low snow years, including greater than 20% during the 2040–2069 period and 50% during the 2070–2099 period. (The simulated change in extremely low years is very similar between March and the other cold-season months; Supplementary Fig. S4.)

The mean changes in low snow years are greater than twice the inter-model and intra-model standard deviation over much of North America, western Eurasia, southeastern Eurasia and northeastern Eurasia beginning in the 2040–2069 period (Fig. 2 and Supplementary Figs S7 and S8). Furthermore, the mean changes in extremely low years are greater than the inter-model standard deviation—and greater than twice the intra-model standard deviation—over much of North America, western Eurasia

[1]Department of Environmental Earth System Science and Woods Institute for the Environment, Stanford University, 473 Via Ortega Stanford, California 94305-4216, USA, [2]Climate Change Science Institute, Oak Ridge National Laboratory, One Bethel Valley Road, Oak Ridge, Tennessee 37831-6301, USA. *e-mail: diffenbaugh@stanford.edu.

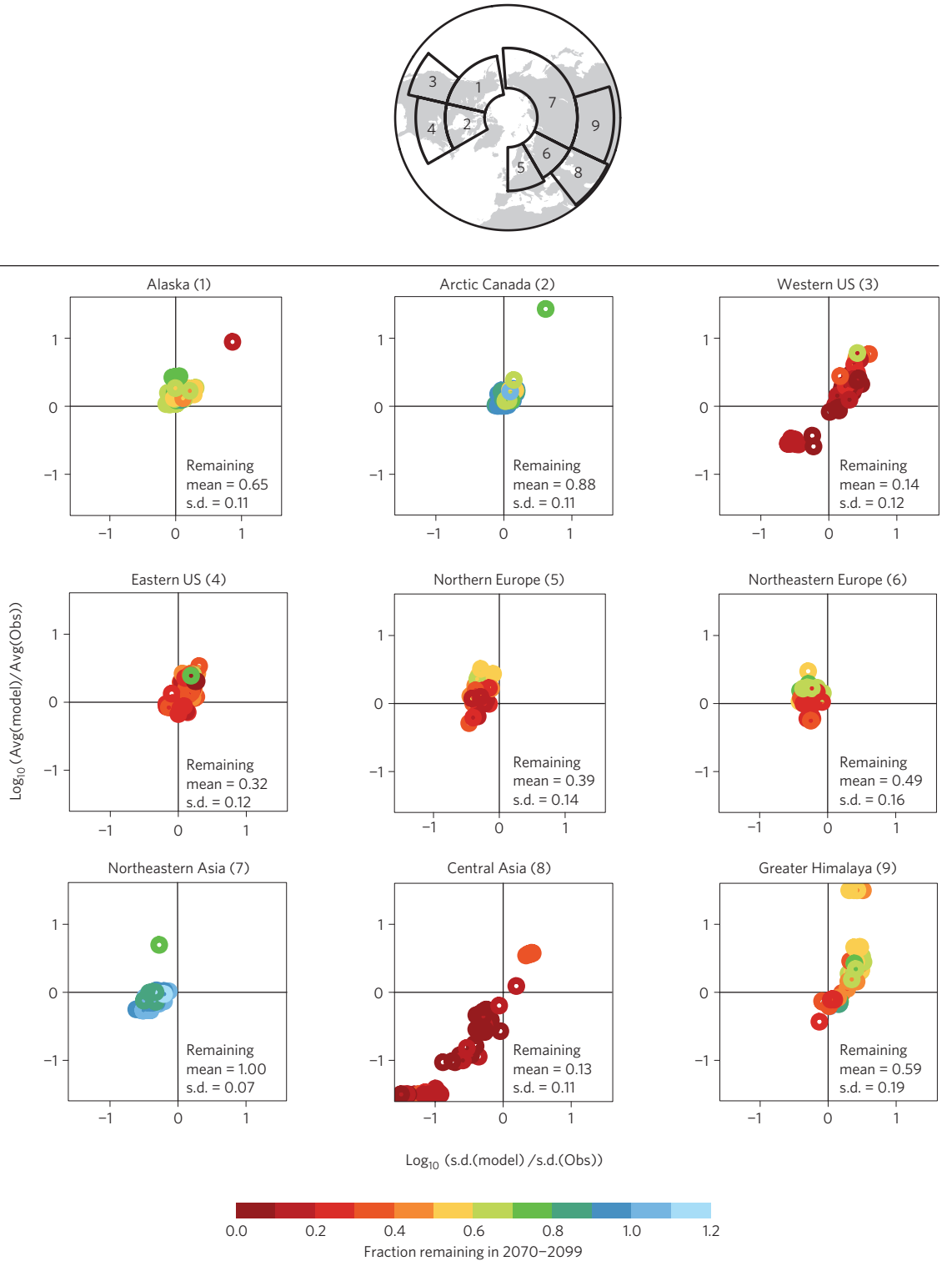

Figure 1 | Comparison of model realizations in the baseline and late-twenty-first-century periods. Each circle shows an individual realization (56 realizations from 26 models; Supplementary Table S1), plotted against that realization's agreement with the observational mean and interannual variability of March SWE in the 1979–2005 period. Colours show the fraction of 1976–2005 March SWE remaining in the 2070–2099 period of RCP 8.5. The agreement in the fractional change in March SWE between the 56 realizations is measured by the mean and standard deviation of the 2070–2099 values (reported in the bottom right of each panel; see Supplementary Table S2 for regional boundaries).

and southeastern Eurasia beginning in the 2040–2069 period (Fig. 2 and Supplementary Figs S7 and S9). In addition to the general pattern of increasing model agreement later in the RCP8.5 pathway, we find generally greater model agreement at common levels of warming (Supplementary Fig. S6) than at common levels of forcing (Fig. 2), suggesting that some of the model differences within each of the RCP8.5 periods (Figs 1 and 2) are due to differences in global climate sensitivity.

Northeastern Eurasia and the high Arctic of North America exhibit both a decreasing occurrence of low snow years (Fig. 2)

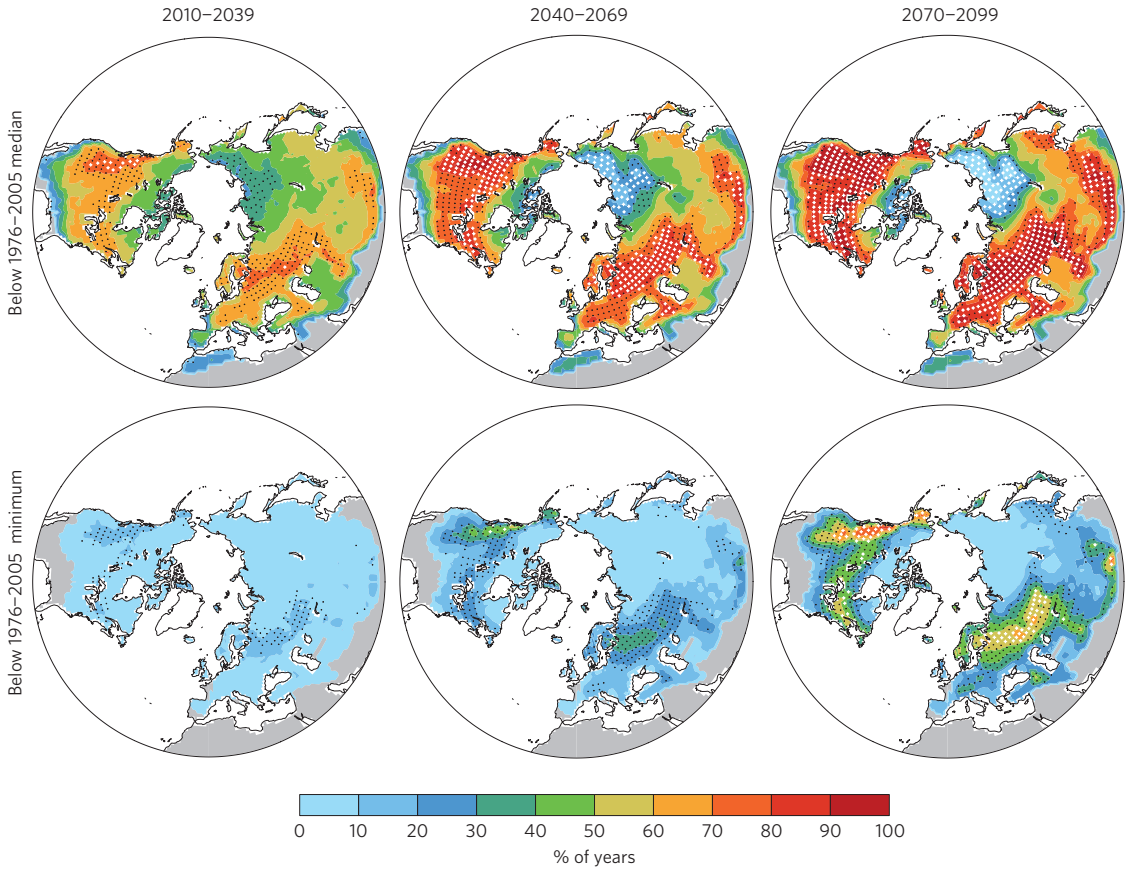

Figure 2 | Emergence of low and extremely low snow years in the twenty-first century. Percentage of years with accumulated March SWE below the simulated 1976–2005 median (top) or minimum (bottom) in three periods of RCP 8.5 (56 realizations from 26 models; Supplementary Table S1). Following ref. 21, stippling indicates areas where the magnitude of the multi-model ensemble mean occurrence divided by the multi-model standard deviation of occurrence exceeds 1.0 (black symbols) or 2.0 (white symbols). Grey denotes areas where at least half of the realizations have a median (top) or minimum (bottom) March SWE of zero in the 1976–2005 period.

and an increasing occurrence of extremely high snow years (Supplementary Fig. S5). The regional increases in high snow years result from increasing precipitation (Fig. 3)[21] in combination with cold-season temperatures that remain below freezing despite twenty-first-century warming[22]. The increasing precipitation is consistent with the response of Arctic water vapour and cloud cover to atmospheric warming[21,22], the response of the Arctic boundary layer inversion to decreasing Arctic sea ice[22], and the response of the dominant storm tracks to a decreased equator-to-pole temperature gradient[23].

The increasing occurrence of low snow years that is identified over much of the Northern Hemisphere (Fig. 2) is associated with substantial changes in the seasonal distribution of total surface runoff (Fig. 3 and Supplementary Figs S10 and S11). For example, the occurrence of years with winter runoff above the simulated baseline winter maximum exceeds 20% in the 2040–2069 period (Supplementary Fig. S11) and 40% in the 2070–2099 period over large areas of North America and Eurasia, with the ensemble mean occurrence exceeding the ensemble standard deviation over most areas of peak occurrence (Fig. 3). In addition, areas of extremely high winter runoff are associated with extremely low spring runoff, including greater than 30% of years below the spring baseline minimum over large areas of western North America and northwestern Eurasia in the 2070–2099 period (Fig. 3). Likewise, the occurrence of extremely high spring runoff exceeds 20% in the 2040–2069 period (Supplementary Fig. S11) and 30% in the 2070–2099 period over the Greater Himalaya[24] and high-latitude areas of North America and northeastern Eurasia (Fig. 3). The extremely high spring runoff over many of these areas is associated with extremely low summer runoff, including greater than 20% of years below the baseline summer minimum over areas of the Greater Himalaya and northeastern Eurasia during the 2070–2099 period. The ensemble mean occurrence of extremely low spring and summer runoff exceeds the ensemble standard deviation primarily in areas of peak occurrence (Fig. 3).

The changes in extreme seasonal total surface runoff seem to be more closely associated with changes in extreme seasonal snowmelt than changes in extreme seasonal precipitation, although extremely high spring precipitation does seem to contribute to the occurrence of extremely high spring total surface runoff over the Greater Himalaya (Fig. 3). Similarly, the occurrence of extremely high spring snowmelt and total surface runoff over northeastern Eurasia in the 2070–2099 period (Fig. 3) is probably due to the occurrence of extremely high March SWE (Supplementary Fig. S5), which is in turn linked to the occurrence of extremely high winter precipitation (Fig. 3). High levels of model agreement are more widespread for extreme precipitation and snowmelt than for extreme total surface runoff (Fig. 3). (Comparisons between precipitation, snowmelt and total surface runoff should be treated with some caution as the CMIP5 data set varies at present in ensemble size for these variables; Supplementary Table S1.)

The model biases (Fig. 1) create a number of important caveats. First, it is important to emphasize that the general circulation models (GCMs) do not resolve the complex topography of the snow-dominated mountain regions. Indeed, the western US, central

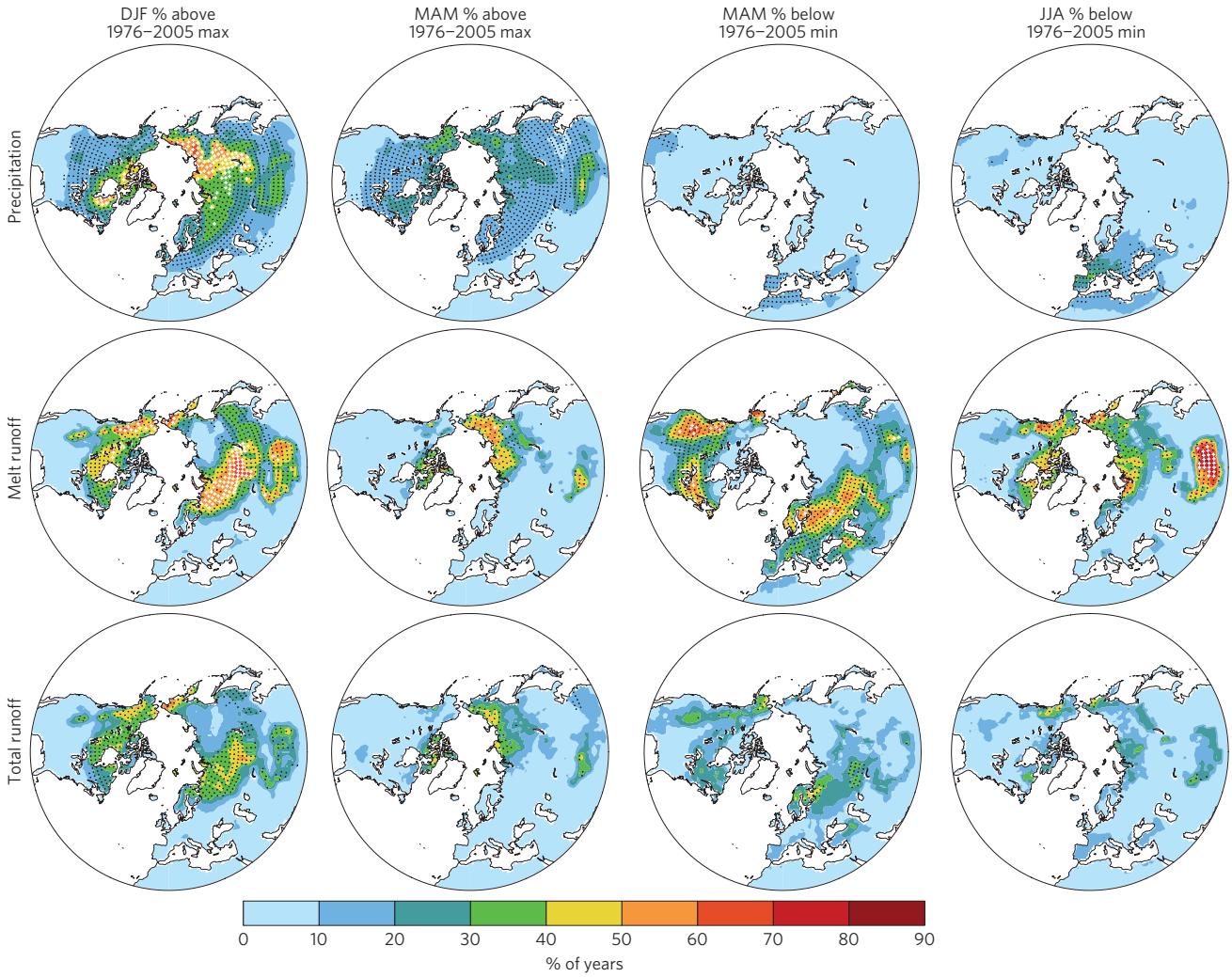

Figure 3 | Emergence of extreme precipitation, melt and runoff years in the twenty-first century. Percentage of years in the 2070–2099 period of the RCP8.5 simulations in which seasonal precipitation (69 realizations from 31 models; Supplementary Table S1), snowmelt runoff (34 realizations from 17 models) or total surface runoff (56 realizations from 27 models) falls below the simulated 1976–2005 seasonal minimum or above the simulated 1976–2005 seasonal maximum. Following ref. 21, stippling indicates areas where the magnitude of the multi-model ensemble mean occurrence divided by the multi-model standard deviation of occurrence exceeds 1.0 (black symbols) or 2.0 (white symbols).

Asia and Greater Himalaya show the greatest variation in model agreement with observations. All three of these regions are both topographically complex (which increases model temperature and precipitation biases through disagreement between the model topography and the real topography) and located in the mid-latitudes (which increases the likelihood that model biases place the simulated cold-season temperature on the incorrect side of the melt-freeze threshold). The western US and Greater Himalaya both exhibit intra-regional heterogeneity in the sign of trends in accumulated solid water over recent decades[6,7], raising particular caution about the ability of GCMs that do not capture the regional topographic complexity to accurately simulate the response of snow-related extremes. However, although the limitations caused by low model resolution should not be under-emphasized, it is notable that most CMIP5 GCMs exhibit higher-than-observed mean and variability of March SWE over the western US and Greater Himalaya during the baseline period (Fig. 1), neither of which would be expected to bias those models towards accelerated increases in extremely low snow accumulation. In contrast, most CMIP5 GCMs exhibit lower-than-observed mean and variability of March SWE over central Asia (Fig. 1), suggesting that the simulated regional reductions in snow accumulation could be artificially enhanced by the model biases. Using bias-corrected and spatially downscaled temperature and precipitation fields from the GCMs as inputs to a hydrologic model would probably improve the agreement between simulated and observed SWE (ref. 25).

Uncertainties associated with precipitation also create important caveats. In particular, as long as temperatures remain sufficiently cold to support solid water, changes in precipitation should dominate the snow response to global warming. The occurrence of extremely high winter precipitation increases over large areas of the high latitudes of North America and Eurasia beginning in the 2040–2069 period, with the ensemble mean exceeding the ensemble standard deviation over most of those areas (Fig. 3 and Supplementary Fig. S11). However, only northeastern Eurasia and areas of the high Arctic of central North America exhibit an increasing occurrence of extremely high cold-season SWE (Supplementary Fig. S5), suggesting that increases in cold-season temperature overwhelm robust increases in extremely high winter precipitation to prevent increases in extremely high snow years over much of the high latitudes. Likewise, the western US—where the temperature is, at present, much closer to the liquid/solid threshold—exhibits increases in extremely low cold-season SWE

(Supplementary Fig. S4), despite increases in extremely high winter precipitation (Fig. 3 and Supplementary Fig. S11). The ensemble mean occurrences of low snow years and high precipitation years exceed the ensemble standard deviation over most areas of the western US (Fig. 3 and Supplementary Figs S4 and S11), again suggesting that increasing cold-season temperatures overwhelm robust increases in the occurrence of extremely high cold-season precipitation. However, unrealistically smooth model topography over the western US could artificially accentuate the influence of warming by artificially raising the simulated surface temperature of high elevation areas, again highlighting the importance of bias correction, spatial downscaling and hydrologic modelling[25]. (Furthermore, when considering our measures of climate model agreement, it is important to note that the different models are not entirely independent[26].)

These caveats notwithstanding, the emergence of frequent snow-related hydrologic extremes could have important impacts, particularly given present reservoir capacity and population growth[1]. For example, the water systems of the western US are heavily dependent on natural storage by mountain snowpack during the cold season and gradual release by snowmelt during the warm season[3]. An increasing occurrence of extremely low snow years (Fig. 2) and a shift towards extremely high winter runoff and extremely low spring runoff (Fig. 3) would increase the need for both flood control and liquid storage capacity, and decrease the availability of water for high-value agricultural systems during the dry warm-season months (when irrigation demand is highest). Early spring snowmelt has also been associated with an increased occurrence of wildfires[9], increased vulnerability of riparian ecosystems[12], enhanced pest pressure[8] and species extinctions[27] in the western US, and similar impacts have been identified in Europe[2,11,13]. Furthermore, >50% of the world's population lives downstream of the Greater Himalaya region[1], with snowmelt providing >40% of pre- and early-monsoon discharge in the Greater Himalaya catchments, and >65% and >30% of annual discharge in the Indus and Tsangpo/Brahmaputra catchments, respectively[24]. An increasing occurrence of extremely low snow years (Fig. 2) and a shift towards extremely high winter/spring runoff and extremely low summer runoff (Fig. 3) would therefore increase the flood risk during the winter/spring, and decrease the availability of freshwater during the summer.

Given the potential impacts across the Northern Hemisphere, our results highlight the likelihood of intensifying hydrologic stress in snow-dependent regions, beginning in the near-term decades when global warming is likely to remain within 2 °C of the pre-industrial baseline[18].

Methods

Models and analysis We analyse global climate model output from the CMIP5 RCP8.5 experiment[16] (Supplementary Table S1). We analyse changes from the 1976 to 2005 baseline in the 2010–2039, 2040–2069 and 2070–2099 periods of RCP8.5, and as a function of global warming in each individual realization. Following ref. 28, we first interpolate each model to a common 1° geographical grid.

We analyse the CMIP5 snw variable, which is defined as the surface snow amount in units of kilograms per square metre. As 1 April SWE is a representative metric of the net snow accumulated during the Northern Hemisphere winter snow season[7,19,20], we focus our analyses on March snw, which reflects the mean monthly March SWE. (Our analyses yield similar SWE results for the other cold-season months; Supplementary Figs S4 and S5.)

We compare the simulated SWE values with observational SWE values from the National Snow and Ice Data Center's global monthly EASE-grid SWE data[29]. The observational snow data are derived from microwave soundings and provided on a 25-km equal area grid. We compare the simulated and observational mean and interannual variability for each model realization over nine Northern Hemisphere regions[30] (Fig. 1 and Supplementary Table S2). We first calculate the area-weighted mean for March of each year in the 1979–2005 period of each model realization and of the observational data set, and then calculate the regional mean and interannual standard deviation of each time series. In addition, we compare the fractional change in regional accumulated March SWE among the different models in the three periods of RCP8.5.

We also analyse the occurrence of the simulated baseline median and minimum accumulated March SWE at each grid point. We first calculate the simulated median and minimum March values at each grid point during the 1976–2005 period of each realization. We then calculate the number of years with March values less than the respective realization median and minimum baseline values at each grid point during the 2010–2039, 2040–2069 and 2070–2099 periods of each realization, and for the 30 years centred on 2 °C, 3 °C and 4 °C of global warming above the pre-industrial baseline. We then calculate the mean of the exceedances across the realizations in each period.

We also analyse the precipitation, snowmelt runoff and total surface runoff during the Northern Hemisphere winter (December–January–February; DJF), spring (March–April–May; MAM), and summer (June–July–August; JJA) seasons. For each of the seasons, we calculate the maximum (minimum) simulated baseline value at each grid point in each realization as the highest (lowest) seasonal value that occurred during the 1976–2005 period. We then calculate the number of seasons with simulated values greater (less) than the respective realization maximum (minimum) baseline value at each grid point during the 2010–2039, 2040–2069 and 2070–2099 periods of each realization. We then calculate the mean of the exceedances across the realizations.

Statistical robustness We calculate five measures of statistical robustness. To quantify the signal-to-noise ratio between the CMIP5 realizations, we follow the Intergovernmental Panel on Climate Change[21] and calculate the ratio between the mean of the model simulated values in the future period and the standard deviation of the model simulated values in the future period, for all of the available realizations (Supplementary Table S1; Measure 1). To test the influence of non-uniform ensemble size on the ensemble signal-to-noise ratio, we repeat Measure 1 using only one realization from each model (Supplementary Table S1; Measure 2). To test the influence of intra-model variability on the ensemble signal-to-noise ratio, we repeat Measure 1 using only the realizations from the individual model that has the largest ensemble size (CSIRO-Mk3-6-0; 10 realizations; Supplementary Table S1; Measure 3).

To test whether the distribution of threshold exceedances in the future period is statistically distinguishable from the distribution resulting from baseline internal climate system variability, we calculate the ratio between the single-model mean occurrence in the future period and the single-model standard deviation of occurrence in the baseline period, using only the realizations from the individual model that has the largest ensemble size (CSIRO-Mk3-6-0). We calculate the single-model standard deviation in the baseline period by first calculating the mean of the 1976–2005 threshold values in the CSIRO-Mk3-6-0 simulations, and then calculating the standard deviation of the distribution of exceedances of that mean threshold across the 10 baseline realizations. We calculate the threshold occurrence in the future period of each CSIRO-Mk3-6-0 realization as in Measure 3 (using the respective historical threshold value from each CSIRO-Mk3-6-0 realization; Measure 4), and using the mean of the historical threshold values from the CSIRO-Mk3-6-0 realizations (Measure 5).

For all five measures, we first subtract the fractional occurrence in the baseline period from the fractional occurrence in the future period. By definition, for the baseline period, the fractional occurrence of years below the baseline median is 0.5, whereas the fractional occurrence of years below the baseline minimum (above the baseline maximum) is 0.0.

Received 9 May 2012; accepted 2 October 2012; published online 11 November 2012

References

1. Barnett, T. P., Adam, J. C. & Lettenmaier, D. P. Potential impacts of a warming climate on water availability in snow-dominated regions. *Nature* **438,** 303–309 (2005).
2. Viviroli, D., Durr, H. H., Messerli, B., Meybeck, M. & Weingartner, R. Mountains of the world, water towers for humanity: Typology, mapping, and global significance. *Wat. Resour. Res.* **43,** 1–13 (2007).
3. Stewart, I. T. Changes in snowpack and snowmelt runoff for key mountain regions. *Hydrol. Process.* **23,** 78–94 (2009).
4. Barnett, T. P. *et al.* Human-induced changes in the hydrology of the western United States. *Science* **319,** 1080–1083 (2008).
5. Choi, G., Robinson, D. A. & Kang, S. Changing Northern Hemisphere snow seasons. *J. Clim.* **23,** 5305–5310 (2010).
6. Gardelle, J., Berthier, E. & Arnaud, Y. Slight mass gain of Karakoram glaciers in the early twenty-first century. *Nature Geosci.* **5,** 322–325 (2012).
7. Mote, P. W., Hamlet, A. F., Clark, M. P. & Lettenmaier, D. P. Declining mountain snowpack in western north America. *Bull. Am. Meteorol. Soc.* **86,** 39–49 (2005).
8. Kurz, W. A. *et al.* Mountain pine beetle and forest carbon feedback to climate change. *Nature* **452,** 987–990 (2008).

9. Westerling, A. L., Hidalgo, H. G., Cayan, D. R. & Swetnam, T. W. Warming and earlier spring increase western US forest wildfire activity. *Science* **313,** 940–943 (2006).
10. Kelly, A. E. & Goulden, M. L. Rapid shifts in plant distribution with recent climate change. *Proc. Natl Acad. Sci. USA* **105,** 11823–11826 (2008).
11. Gornall, J. *et al.* Implications of climate change for agricultural productivity in the early twenty-first century. *Phil. Trans. R. Soc. B* **365,** 2973–2989 (2010).
12. Rood, S. B. *et al.* Declining summer flows of Rocky Mountain rivers: Changing seasonal hydrology and probable impacts on floodplain forests. *J. Hydrol.* **349,** 397–410 (2008).
13. Schroter, D. *et al.* Ecosystem service supply and vulnerability to global change in Europe. *Science* **310,** 1333–1337 (2005).
14. Cayan, D. R. Interannual climate variability and snowpack in the western United States. *J. Clim.* **9,** 928–948 (1996).
15. Scherrer, S. C. & Appenzeller, C. Swiss Alpine snow pack variability: Major patterns and links to local climate and large-scale flow. *Clim. Res.* **32,** 187–199 (2006).
16. Taylor, K. E., Stouffer, R. J. & Meehl, G. A. An overview of CMIP5 and the experiment design. *Bull. Am. Meteorol. Soc.* **93,** 485–498 (2012).
17. Moss, R. H. *et al.* The next generation of scenarios for climate change research and assessment. *Nature* **463,** 747–756 (2010).
18. Rogelj, J., Meinshausen, M. & Knutti, R. Global warming under old and new scenarios using IPCC climate sensitivity range estimates. *Nature Clim. Change* **2,** 248–253 (2012).
19. Kapnick, S. & Hall, A. Causes of recent changes in western North American snowpack. *Clim. Dyn.* **38,** 1885–1899 (2011).
20. Bohr, G. S. & Aguado, E. Use of April 1 SWE measurements as estimates of peak seasonal snowpack and total cold-season precipitation. *Wat. Resour. Res.* **37,** 51–60 (2001).
21. Meehl, G. A. in *IPCC Climate Change 2007: The Physical Science Basis* (eds Solomon, S. *et al.*) Ch. 10 (Cambridge Univ. Press, 2007).
22. Deser, C., Tomas, R., Alexander, M. & Lawrence, D. The seasonal atmospheric response to projected Arctic sea ice loss in the late twenty-first century. *J. Clim.* **23,** 333–351 (2010).
23. Yin, J. H. A consistent poleward shift of the storm tracks in simulations of 21st century climate. *Geophys. Res. Lett.* **32,** L18701 (2005).
24. Bookhagen, B. & Burbank, D. W. Toward a complete Himalayan hydrological budget: Spatiotemporal distribution of snowmelt and rainfall and their impact on river discharge. *J. Geophys. Res.* **115,** F03019 (2010).
25. Ashfaq, M., Bowling, L. C., Cherkauer, K., Pal, J. S. & Diffenbaugh, N. S. Influence of climate model biases and daily-scale temperature and precipitation events on hydrological impacts assessment: A case study of the United States. *J. Geophys. Res.* **115,** D14116 (2010).
26. Masson, D. & Knutti, R. Climate model genealogy. *Geophys. Res. Lett.* **38,** L08703 (2011).
27. Boggs, C. L. & Inouye, D. W. A single climate driver has direct and indirect effects on insect population dynamics. *Ecol. Lett.* **15,** 502–508 (2012).
28. Diffenbaugh, N. S. & Scherer, M. Observational and model evidence of global emergence of permanent, unprecedented heat in the 20th and 21st centuries. *Clim. Change* **107,** 615–624 (2011).
29. Armstrong, R. L., Brodzik, M. J., Knowles, K. & Savoie, M. *Global Monthly EASE-Grid Snow Water Equivalent Climatology* (National Snow and Ice Data Center, Digital Media, 2007).
30. Giorgi, F. & Bi, X. Updated regional precipitation and temperature changes for the 21st century from ensembles of recent AOGCM simulations. *Geophys. Res. Lett.* **32,** L21715 (2005).

Acknowledgements

Support for data storage and analysis was provided by the Center for Computational Earth and Environmental Sciences in the School of Earth Sciences at Stanford University. We acknowledge the World Climate Research Programme's Working Group on Coupled Modelling, which is responsible for CMIP, and we thank the climate modelling groups (listed in Supplementary Table S1) for producing and making available their model output. For CMIP the US Department of Energy's Program for Climate Model Diagnosis and Intercomparison provides coordinating support and led development of software infrastructure in partnership with the Global Organization for Earth System Science Portals. We thank the National Snow and Ice Data Center for providing the SWE data. Our work was supported by NSF award 0955283 and NIH award 1R01AI090159-01 to N.S.D., and ORNL LDRD 32112413 and DOE award ERKP777 to M.A.

Author contributions

N.S.D. designed the climate model analysis, performed the climate model analysis and wrote the paper. M.S. designed the climate model analysis and performed the climate model analysis. M.A. designed the climate model analysis and wrote the paper.

Additional information

Supplementary information is available in the online version of the paper. Reprints and permissions information is available online at www.nature.com/reprints. Correspondence and requests for materials should be addressed to N.S.D.

Competing financial interests

The authors declare no competing financial interests.